Metal-Organic Frameworks Hot Paper

Deutsche Ausgabe: DOI: 10.1002/ange.201904160
Internationale Ausgabe: DOI: 10.1002/anie.201904160

Induced Fit of C_2H_2 in a Flexible MOF Through Cooperative Action of Open Metal Sites

Heng Zeng, Mo Xie, Yong-Liang Huang, Yifang Zhao, Xiao-Jing Xie, Jian-Ping Bai, Meng-Yan Wan, Rajamani Krishna, Weigang Lu, and Dan Li**

Abstract: *Porous materials that can undergo pore-structure adjustment to better accommodate specific molecules are ideal for separation and purification. Here, we report a stable microporous metal-organic framework, JNU-1, featuring one-dimensional diamond-shaped channels with a high density of open metal sites arranged on the surface for the cooperative binding of acetylene. Together with its framework flexibility and appropriate pore geometry, JNU-1 exhibits an induced-fit behavior for acetylene. The specific binding sites and continuous framework adaptation upon increased acetylene pressure are validated by molecular modeling and in situ X-ray diffraction study. This unique induced-fit behavior endows JNU-1 with an unprecedented increase in the acetylene binding affinity (adsorption enthalpy: up to 47.6 kJ mol^{-1} at ca. 2.0 mmol g^{-1} loading).*

Molecular recognition by induced fit is at the heart of all biological processes.[1] It is a key event in signal transduction,[2] site activation,[3] and allosteric regulation.[4] One prominent example is enzyme–substrate complex formation, which, as Koshland[1a] proposed in 1958, may occur via an induced-fit process. An enzyme can adjust its shape by interacting with a substrate, resulting in a pocket specifically for the substrate to dock (Scheme 1); therefore, the active site of the enzyme can perform a maximum catalytic function. Supramolecular cages with a similar binding effect in solution have been reported before;[5] however, it is challenging to develop porous solid materials to mimic such an induced-fit behavior for molecular recognition, which would be desired for many large-volume applications including industrial gas purification.

Acetylene (C_2H_2) is an important starting material for many chemical[6] and electronic[7] products. Yet, it is very reactive and may cause unwanted chemical reactions. Steam cracking of hydrocarbons is the primary method for producing lighter alkenes and C_2H_2 is an inevitable byproduct.[8] Recent studies have revealed that a number of metal-organic frameworks[9] (MOFs) show an increased C_2H_2 selectivity over other gas molecules through ligand functionalization,[10] pore size/shape customization,[11] surface polarization,[12] and, in particular, open-metal-sites incorporation.[13] The latter usually contributes more to the binding affinity because of the ability of C_2H_2 to coordinate to the metal center. However, most of the MOF materials studied for C_2H_2 selectivity have rigid frameworks whose dimensions barely change upon C_2H_2 loading, which inevitably results in a decrease in binding affinity once the strongest adsorption sites for C_2H_2 are occupied.

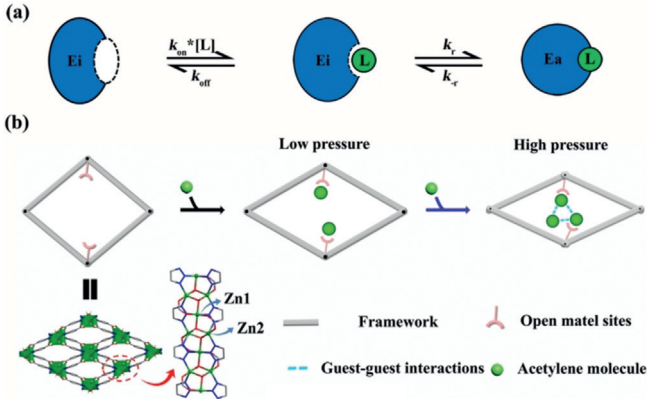

Scheme 1. a) Illustration of the induced-fit mechanism in substrate–enzyme binding. b) Schematic representation of a continuous directional contraction upon C_2H_2 adsorption in JNU-1.

To mimic an enzyme-like behavior, flexible MOFs whose scaffolds can self-adapt to match the size of the guest molecules are of particular interest. The initially confined guest molecules may induce a continuous and directional shrinkage of the framework so that the guests can fit more tightly, rendering a progressively enhanced host–guest interaction, that is, an increased binding affinity. This induced-fit behavior in MOF materials has rarely been explored. Herein, we report such a flexible MOF exhibiting an unprecedented increase in binding affinity for C_2H_2. Experimental results and theoretical models reveal that this induced-fit effect is realized through the cooperative action of open metal sites.

A microporous MOF, $[Zn_3(OH)_2(btca)_2]$ (in the following referred to as JNU-1, H_2btca = benzotriazole-5-carboxylic acid), was synthesized according to the reported procedure,[14] and it was selected for this study because of the framework flexibility and high density of open metal sites (OMS) (Figures S1 and S2, Supporting Information). The critical role of OMS in enhancing the sorbate binding affinity in MOF materials has been well established,[15] and the potential OMS

[*] H. Zeng, Dr. M. Xie, Dr. Y. L. Huang, Dr. Y. Zhao, X. J. Xie, J. P. Bai, M. Y. Wan, Prof. Dr. W. Lu, Prof. Dr. D. Li
College of Chemistry and Materials Science, Jinan University
Guangzhou 510632 (P. R. China)
E-mail: weiganglu@jnu.edu.cn
danli@jnu.edu.cn
Prof. Dr. R. Krishna
Van't Hoff Institute for Molecular Sciences, University of Amsterdam
Science Park 904, 1098 XH Amsterdam (The Netherlands)
Supporting information and the ORCID identification number(s) for the author(s) of this article can be found under: https://doi.org/10.1002/anie.201904160.

density in JNU-1 was calculated to be 3.2 nm^{-3} by counting the number of OMS per unit cell volume, which is comparable to benchmark OMS-based MOF sorbents such as Mg-MOF-74 (4.6 nm^{-3}), HKUST-1 (2.6 nm^{-3}), and UTSA-74 (2.5 nm^{-3}). It is worth noting that one third of the zinc centers in JNU-1 and half in UTSA-74 are fully coordinated in octahedral geometries without labile coordinating solvents necessary for creating OMS.[16] As shown in Scheme 1, JNU-1 is a three-dimensional (3D) framework featuring one-dimensional (1D) diamond-shaped channels. Each asymmetric unit consists of two crystallographically independent Zn^{II} sites: Zn1 in an octahedral coordination mode and Zn2 in a distorted square-pyramidal coordination mode (Figure S2). Because of the absence of coordinative saturation and the spatial proximity, two neighboring Zn2 atoms may be able to bind one guest molecule cooperatively. Furthermore, the activated JNU-1 is non-porous along the *a* and *b* axes, whereas it exhibits microporous channels of ca. 8 Å diameter along the *c* axis with the zinc OMS pointing to the channel centers. This arrangement suggests an easy access to OMS and the possibility of multiple host–guest/guest–guest interactions.

The phase purity of bulk JNU-1 was determined by the comparison of the simulated and experimental powder X-ray Diffraction (PXRD) patterns (Figure S3). It is stable in water over a pH range of 2 to 12, as evidenced by the retained peaks and relative intensities in the corresponding PXRD patterns (Figure 1 d) as well as the retained porosity (Figure S6). Thermogravimetric analysis (TGA) revealed that JNU-1 is thermally stable up to 450 °C in a N_2 atmosphere (Figure S7), which is consistent with in situ variable-temperature PXRD investigations (Figure S4). The permanent porosity of JNU-1 was confirmed by N_2 sorption isotherms at 77 K (Figure S5) and it showed a type-I isotherm with a calculated Brunauer–Emmett–Teller (BET) surface area of 818 $m^2 g^{-1}$. Note that the sample was activated under high vacuum at 200 °C for 36 h without any prior solvent exchange.

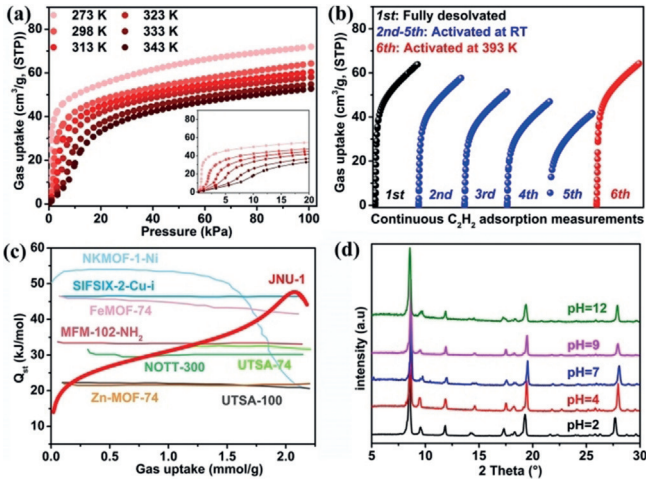

Figure 1. a) C_2H_2 adsorption isotherms for JNU-1 at different temperatures (inset: zoomed in to highlight the adsorption steps at low pressures and low temperatures). b) Continuous C_2H_2 adsorption measurements of JNU-1 at 298 K, the sample was fully desolvated (1st measurement), and activated at room temperature (2nd to 5th) and at 393 K (6th). c) C_2H_2 adsorption enthalpy (Q_{st}) of JNU-1 and some selected MOFs, note the increasing Q_{st} for JNU-1. d) PXRD patterns of JNU-1 after being immersed in different pH solutions for 24 h.

C_2H_2 adsorption data were collected for the activated JNU-1 at different temperatures (Figure 1 a). The isotherms displayed adsorption steps at low pressures that gradually disappeared with the increase of temperature (Inset in Figure 1 a). Step-shaped gas adsorption phenomena have been frequently observed in chemisorption on mmen-M_2-(dobpdc) and some flexible MOFs, particularly for CO_2,[17,18] but they are not common in physisorption. This suggests a strong interaction with C_2H_2. After the C_2H_2 adsorption measurement with fully desolvated JNU-1 (1st in Figure 1 b), the same sample was activated on a ASAP2020 Plus instrument at room temperature (pumped at 5 μmHg for 0.5 h) and the C_2H_2 adsorption was measured again. The activation/measurement cycle was repeated several times (2nd to 5th in Figure 1 b). A continuous decrease in the adsorption capacity was observed, which is hardly seen in physisorption processes, indicating an unusually strong binding for C_2H_2. The initial C_2H_2 adsorption capacity can be fully restored if activated at a higher temperature (6th in Figure 1 b).

The adsorption enthalpy (Q_{st}) is a quantitative measurement of the binding affinity. The Q_{st} for JNU-1 lies within a range of 13 to 47.6 kJ mol^{-1} (Figure 1 c). Strikingly, the Q_{st} value increases with C_2H_2 loading, which, to the best of our knowledge, has rarely been reported before, implying a progressively stronger host–guest interaction.[19] The maximum Q_{st} for JNU-1 is 47.6 kJ mol^{-1}, comparable to those for TIFSIX-2-Cu-i (46.2 kJ mol^{-1})[20] and FeMOF-74 (47 kJ mol^{-1}),[13] and only slightly lower than that for NKMOF-1-M (M = Cu or Ni) (Figures 1 c and S13).[21] Note that the maximum Q_{st} for JNU-1 is at 2.0 mmol g^{-1} of C_2H_2 loading, whereas other MOFs are usually at zero loading. Additionally, the maximum Q_{st} for JNU-1 is the highest among all reported MOFs with open Zn^{II} sites, including UTSA-74[22] and Zn-MOF-74,[23] indicative of a superior binding affinity of JNU-1 towards C_2H_2, possibly due to the cooperative action of two open Zn^{II} sites on one C_2H_2 molecule.

To understand the unusual but excellent C_2H_2 binding affinity of JNU-1, in situ C_2H_2 adsorption experiments coupled with PXRD measurements were performed.[24] Upon C_2H_2 adsorption, significant changes in the PXRD patterns were observed (Figures 2 a and S18). A continuous

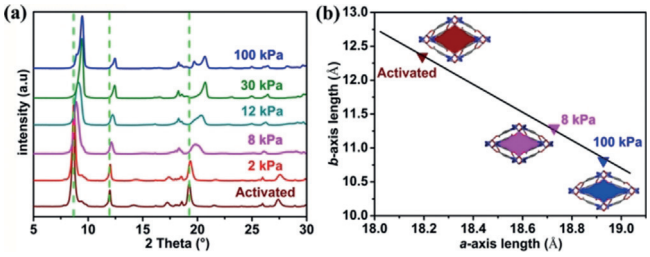

Figure 2. a) In situ PXRD patterns of JNU-1 in different C_2H_2 concentrations balanced by N_2. b) Variation of the unit cell parameters *a* and *b* over C_2H_2 pressure. Insets show top views of the channel at the indicated C_2H_2 pressure.

shift of peaks, especially the two indexed as (110) and (111), to higher angles suggests that the framework can self-adapt in response to the increasing loading of C_2H_2 (Figure S18). In flexible MOFs, it is generally expected that the framwork adopts a closed form upon desolvation and restores its open form by guest intrusion. JNU-1, however, exhibits a very different behavior in the second step; it adopts a more closed form instead of opening up upon C_2H_2 adsorption (Figure 3a). To verify this unique behavior of JNU-1, molecular

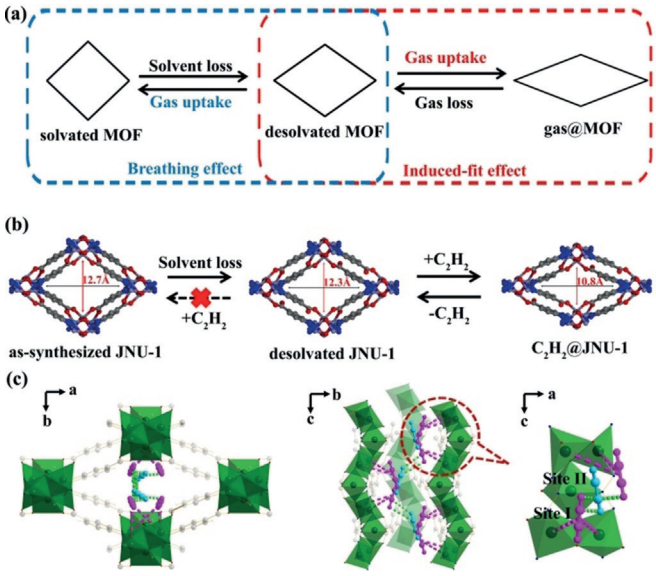

Figure 3. a) Schematic comparison of the breathing and induced-fit effect. Note the change in the channel geometry (expansion or shrinkage) upon gas uptake (guests were omitted for clarity). b) Illustration of the induced-fit behavior in JNU-1. Note the continuous channel shrinkage (guests were omitted for clarity). c) Single-crystal structure of C_2H_2@JNU-1 with observed C_2H_2 molecules on site I (pink) and site II (blue).

modeling of the bare JNU-1 structure under different C_2H_2 pressures was performed and the PXRD patterns extracted from the optimized structures are in good agreement with the experimental in situ PXRD patterns under the same pressures (Figure S21). Additionally, the unit-cell parameters of the optimized structures clearly show a continuous shrinkage along the *b* axis upon increasing pressure (Figure 2b). Furthermore, it was confirmed by a single-crystal X-ray diffraction (SCXRD) study that the channel size of JNU-1 along the *b* axis is reduced from 12.7 to 12.3 Å upon desolvation and further reduced to 10.8 Å upon C_2H_2 adsorption (Figure 3b).

To further elucidate the mechanism of the increasing binding affinity for C_2H_2 in JNU-1, we performed detailed theoretical investigations using periodic density functional theory (DFT). In the DFT-optimized bare JNU-1 structure, two independent binding sites (I and II) are apparent: C_2H_2 molecules on site I exhibit side-on interactions with two open Zn^{II} centers, while C_2H_2 molecules on site II interact primarily with two C_2H_2 molecules on two nearby sites I via intermolecular dipole interactions (Figure S21). Two coordinatively unsaturated Zn^{II} centers attract one C_2H_2 molecule and place it on site I through cooperative action. Once all sites of type I are occupied, C_2H_2 molecules start to occupy sites of type II (Figure S22a).

To directly visualize the C_2H_2 molecules in the channel, we carried out SCXRD analysis for C_2H_2@JNU-1, which is JNU-1 preloaded with C_2H_2. First, the desolvated JNU-1 crystals were put in a C_2H_2 atmosphere (C_2H_2 balloon) at room temperature for 6 h; then, SCXRD data were collected at 150 K. In the resolved crystal structure, C_2H_2 molecules were found to simultaneously bond to two open Zn^{II} centers (Figure 3c), consistent with site I determined by molecular modeling. The measured distances from the closest carbon atom of the C_2H_2 molecule to the two Zn^{II} centers are 3.92 and 4.01 Å, indicating strong electrostatic interactions. Fortunately, the C_2H_2 molecule on site II was also identified despite positional disorder. It is located between two C_2H_2 molecules on two nearby sites I with bonding distances (closest carbon atom to Zn^{II} centers) ranging from 4.2 to 4.3 Å (Figure S22b). These results further confirm the induced-fit behavior of JNU-1 and unravel the mechanism of its exceptional C_2H_2 binding affinity.

Adsorption selectivity is a critical factor to assess the separation performance of an adsorbent material.[25] It is generally anticipated that CO_2 will be a more strongly interacting guest than hydrocarbon molecules because of the polarizability. In fact, we discovered that CO_2 could also cause a contraction along the *b* axis in CO_2-loaded crystals at 150 K. Yet, in contrast to C_2H_2-loaded JNU-1, where each C_2H_2 molecule is clearly seen to be bonded to two zinc centers, the CO_2 molecules in CO_2-loaded JNU-1 are highly disordered (Figure S23), indicating a relatively weak host–guest interaction. The results are consistent with the calculated binding affinities for C_2H_2 and CO_2 at high loadings (Figure S17). Thus, the C_2H_2/CO_2 selectivity should be able to confirm if JNU-1 indeed possesses an unusually strong binding affinity for C_2H_2. Compared with other MOFs, the C_2H_2/CO_2 uptake ratio of JNU-1 is 6.6 at 3 kPa (Figure S9), which is among the highest and close to the best-performaning $[Cu_2(pzdc)_2(pyz)]$ (uptake ratio: 10.5 at 4.5 kPa and 270 K).[26] Furthermore, we calculated the selectivity according to the ideal adsorbed solution theory (IAST) for JNU-1. As shown in Figure 4a, the IAST adsorption selectivity at 298 K was determined to be 285.6 for C_2H_2/CO_2 (1/1, v/v) at the initial loading, indicating a good selectivity and potential applicability for separating C_2H_2 from CO_2.

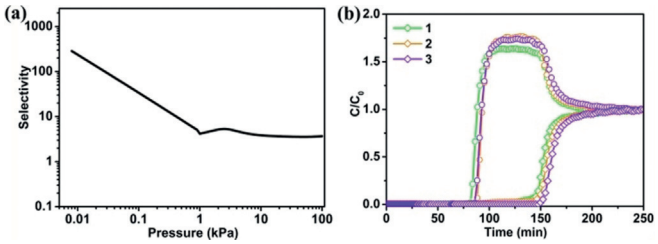

Figure 4. a) Calculated IAST adsorption selectivity of C_2H_2 over CO_2 for JNU-1 in an equimolar mixture of C_2H_2/CO_2 at 298 K. b) Three cycles of experimental column breakthrough curves for JNU-1 in a C_2H_2/CO_2(50/50, v/v) mixture at 298 K. *C* is the gas concentration at the outlet; C_0 is the gas concentration in the feed.

As widely used as it has been in depicting the gas-separation potential, the IAST selectivity from the single-component adsorption isotherms may not necessarily reflect the real separation capability from gas mixtures, especially in flexible MOF materials with gate-opening behavior. To further evaluate the C_2H_2/CO_2 separation performance of JNU-1 in practical adsorption processes, we conducted lab-scale fixed-bed breakthrough tests under ambient conditions. Here, a gas mixture of C_2H_2/CO_2 (50/50, v/v) was introduced over a packed column of activated JNU-1 solid (2.2 g) at a rate of 2.0 mL min^{-1} and 298 K. As shown in Figure 4b, CO_2 was detected after the mixed gas had flowed into the fixed bed for about 75 min, whereas C_2H_2 was not detected until the breakthrough time (150 min). Thus, the C_2H_2 adsorption capacity of JNU-1 was estimated to be 140 mL/2.2 g, which is close to the single-component C_2H_2 adsorption capacity (60 mL g^{-1}). The breakthrough results demonstrate that JNU-1 is highly efficient for the challenging separation of C_2H_2/CO_2 mixtures.

In conclusion, we report that a flexible microporous MOF (JNU-1) exhibits an induced-fit behavior for C_2H_2, as evidenced by an unprecedented increase in adsorption enthalpy with C_2H_2 loading, and further validated by the in situ X-ray diffraction study as well as theoretical modeling. The unusual but excellent C_2H_2 binding affinity originates from the cooperative binding of two unsaturated Zn^{II} centers to one C_2H_2 molecule, followed by a self-adaptive shrinkage of the framework to further enhance the host–guest and guest–guest interactions. Continuous measurements of C_2H_2 adsorption–desorption appears to confirm the extremely strong binding, where C_2H_2 can only be completely removed under a high vacuum and at a high temperature (393 K). Although a large energy penalty would be associated with the regeneration of JNU-1, the building of strong adsorption sites is a general approach to improve the adsorption capacity. Therefore, a balance needs to be struck between the binding affinity and the regeneration energy for the material design in this line of work. The realization of induced fit in this work opens a new direction in designing porous solid materials for molecular recognition.

Acknowledgements

This work was financially supported by the National Natural Science Foundation of China (Nos. 21731002, 91222202).

Conflict of interest

The authors declare no conflict of interest.

Keywords: binding affinity · cooperative action · gas separation · induced fit · porous materials

How to cite: *Angew. Chem. Int. Ed.* **2019**, *58*, 8515–8519
Angew. Chem. **2019**, *131*, 8603–8607

[1] a) D. E. Koshland, Jr., *Proc. Natl. Acad. Sci. USA* **1958**, *44*, 98–104; b) D. E. Koshland, Jr., *Angew. Chem. Int. Ed.* **1994**, *33*, 2375–2378; *Angew. Chem.* **1994**, *106*, 2468–2472; c) S. Hiraoka, M. Fujita, *J. Am. Chem. Soc.* **1999**, *121*, 10239–10240; d) C. Talotta, C. Gaeta, M. De Rosa, J. Ascenso, P. M. Marcos, P. Neri, *Eur. J. Org. Chem.* **2016**, 158–167; e) S. Wang, T. Sawada, K. Ohara, K. Yamaguchi, M. Fujita, *Angew. Chem. Int. Ed.* **2016**, *55*, 2063–2066; *Angew. Chem.* **2016**, *128*, 2103–2106; f) W. Wang, Y.-X. Wang, H.-B. Yang, *Chem. Soc. Rev.* **2016**, *45*, 2656–2693.

[2] a) S. Matile, A. Vargas Jentzsch, J. Montenegro, A. Fin, *Chem. Soc. Rev.* **2011**, *40*, 2453–2474; b) S. Maiti, C. Pezzato, S. Garcia Martin, L. J. Prins, *J. Am. Chem. Soc.* **2014**, *136*, 11288–11291; c) M. J. Langton, L. M. Scriven, N. H. Williams, C. A. Hunter, *J. Am. Chem. Soc.* **2017**, *139*, 15768–15773; d) P. A. Gale, J. T. Davis, R. Quesada, *Chem. Soc. Rev.* **2017**, *46*, 2497–2519; e) I. M. Bennett, H. M. V. Farfano, F. Bogani, A. Primak, P. A. Liddell, L. Otero, L. Sereno, J. J. Silber, A. L. Moore, T. A. Moore, D. Gust, *Nature* **2002**, *420*, 398–401.

[3] R. Domínguez, H. Souchon, M.-B. Lascombe, P. M. Alzari, *J. Mol. Biol.* **1996**, *257*, 1042–1051.

[4] a) L. Kovbasyuk, R. Krämer, *Chem. Rev.* **2004**, *104*, 3161–3187; b) C. G. Oliveri, P. A. Ulmann, M. J. Wiester, C. A. Mirkin, *Acc. Chem. Res.* **2008**, *41*, 1618–1629; c) M. J. Wiester, P. A. Ulmann, C. A. Mirkin, *Angew. Chem. Int. Ed.* **2011**, *50*, 114–137; *Angew. Chem.* **2011**, *123*, 118–142; d) A. J. McConnell, P. D. Beer, *Angew. Chem. Int. Ed.* **2012**, *51*, 5052–5061; *Angew. Chem.* **2012**, *124*, 5138–5148; e) J. Guo, H.-X. Zhou, *Chem. Rev.* **2016**, *116*, 6503–6515; f) A. Faulkner, T. van Leeuwen, B. L. Feringa, S. J. Wezenberg, *J. Am. Chem. Soc.* **2016**, *138*, 13597–13603; g) E. Sevcsik, A. J. Trexler, J. M. Dunn, E. Rhoades, *J. Am. Chem. Soc.* **2011**, *133*, 7152–7158; h) Y. Suzuki, T. Nakamura, H. Iida, N. Ousaka, E. Yashima, *J. Am. Chem. Soc.* **2016**, *138*, 4852–4859.

[5] a) M. Fujita, S. Nagao, K. Ogura, *J. Am. Chem. Soc.* **1995**, *117*, 1649–1650; b) T. Sawada, H. Hisada, M. Fujita, *J. Am. Chem. Soc.* **2014**, *136*, 4449–4451; c) C. M. Hong, D. M. Kaphan, R. G. Bergman, K. N. Raymond, F. D. Toste, *J. Am. Chem. Soc.* **2017**, *139*, 8013–8021; d) Y-Y. Zhan, T. Kojima, T. Nakamura, T. Takahashi, S. Takahashi, Y. Haketa, Y. Shoji, H. Maeda, T. Fukushima, S. Hiraoka, *Nat. Commun.* **2018**, *9*, 4530; e) O. Taratula, P. A. Hill, N. S. Khan, P. J. Carroll, I. J. Dmochowski, *Nat. Commun.* **2010**, *1*, 148; f) S. Hiraoka, K. Harano, T. Nakamura, M. Shiro, M. Shionoya, *Angew. Chem. Int. Ed.* **2009**, *48*, 7006–7009; *Angew. Chem.* **2009**, *121*, 7140–7143; g) K. Kasai, M. Aoyagi, M. Fujita, *J. Am. Chem. Soc.* **2000**, *122*, 2140–2141.

[6] *Modern Acetylene Chemistry* (Eds.: P. J. Stang, F. Diederich), VCH, Weinheim, **1995**.

[7] J. C. W. Chien, *Polyacetylene: Chemistry, Physics, and Material Science*, Academic Press, Orlando, **1984**.

[8] F. A. Henglein, *Chemical Technology*, *1st ed.*, Pergamon, Oxford, **1969**.

[9] a) H. C. Zhou, J. R. Long, O. M. Yaghi, *Chem. Rev.* **2012**, *112*, 673–674; b) H. C. Zhou, S. Kitagawa, *Chem. Soc. Rev.* **2014**, *43*, 5415–5418; c) H. Furukawa, K. E. Cordova, M. O'Keeffe, O. M. Yaghi, *Science* **2013**, *341*, 1230444; d) B. Chen, S. C. Xiang, G. D. Qian, *Acc. Chem. Res.* **2010**, *43*, 1115–1124; e) J. P. Zhang, X. M. Chen, *J. Am. Chem. Soc.* **2009**, *131*, 5516–5521; f) S. Horike, S. Shimomura, S. Kitagawa, *Nat. Chem.* **2009**, *1*, 695–704; g) J. P. Zhang, H. L. Zhou, D. D. Zhou, P. Q. Liao, X. M. Chen, *Natl. Sci. Rev.* **2018**, *5*, 907–919.

[10] T.-L. Hu, H. L. Wang, B. Li, R. Krishna, H. Wu, W. Zhou, Y. F. Zhao, Y. Han, X. Wang, W. D. Zhu, Z. Z. Yao, S. C. Xiang, B. L. Chen, *Nat. Commun.* **2015**, *6*, 7328.

[11] a) R.-B. Lin, L. Li, H. Wu, H. Arman, B. Li, R.-G. Lin, W. Zhou, B. Chen, *J. Am. Chem. Soc.* **2017**, *139*, 8022–8028; b) Y. Ye, Z.

Ma, R-B. Lin, R. Krishna, W. Zhou, Q. Lin, Z. Zhang, S. Xiang, B. Chen, *J. Am. Chem. Soc.* **2019**, *141*, 4130 – 4136.
[12] a) B. Li, X. Cui, D. O'Nolan, H.-M. Wen, M. Jiang, R. Krishna, H. Wu, R.-B. Lin, Y.-S. Chen, D. Yuan, H. Xing, W. Zhou, Q. Ren, G. Qian, M. J. Zaworotko, B. Chen, *Adv. Mater.* **2017**, *29*, 1704210; b) J. Lee, C. Y. Chuah, J. Kim, Y. Kim, N. Ko, Y. Seo, K. Kim, T. H. Bae, E. Lee, *Angew. Chem. Int. Ed.* **2018**, *57*, 7869 – 7873; *Angew. Chem.* **2018**, *130*, 7995 – 7999.
[13] E. D. Bloch, W. L. Queen, R. Krishna, J. M. Zadrozny, C. M. Brown, J. R. Long, *Science* **2012**, *335*, 1606 – 1610.
[14] J. Xiao, Y. Wu, M. Li, B.-Y. Liu, X.-C. Huang, D. Li, *Chem. Eur. J.* **2013**, *19*, 1891 – 1895.
[15] a) M. Dincă, A. Dailly, Y. Liu, C. M. Brown, D. A. Neumann, J. R. Long, *J. Am. Chem. Soc.* **2006**, *128*, 16876 – 16883; b) M. Dincă, W. S. Han, Y. Liu, A. Dailly, C. M. Brown, J. R. Long, *Angew. Chem. Int. Ed.* **2007**, *46*, 1419 – 1422; *Angew. Chem.* **2007**, *119*, 1441 – 1444.
[16] Z. J. Zhang, Y. G. Zhao, Q. H. Gong, Z. Li, J. Li, *Chem. Commun.* **2013**, *49*, 653 – 661.
[17] T. M. McDonald, J. A. Mason, X. Kong, E. D. Bloch, D. Gygi, A. Dani, V. Crocella, F. Giordanino, S. O. Odoh, W. Drisdell, B. Vlaisavljevich, A. L. Dzubak, R. Poloni, S. K. Schnell, N. Planas, K. Lee, T. Pascal, L. F. Wan, D. Prendergast, J. B. Neaton, B. Smit, J. B. Kortright, L. Gagliardi, S. Bordiga, J. A. Reimer, J. R. Long, *Nature* **2015**, *519*, 303 – 308.
[18] a) K. S. Walton, A. R. Millward, D. Dubbeldam, H. Frost, J. J. Low, O. M. Yaghi, R. Q. Snurr, *J. Am. Chem. Soc.* **2008**, *130*, 406 – 407; b) C. Serre, F. Millange, C. Thouvenot, M. Noguès, G. Marsolier, D. Louër, G. Férey, *J. Am. Chem. Soc.* **2002**, *124*, 13519 – 13526; c) M. L. Foo, R. Matsuda, Y. Hijikata, R. Krishna, H. Sato, S. Horike, A. Hori, J. G. Duan, Y. Sato, Y. Kubota, M. Takata, S. Kitagawa, *J. Am. Chem. Soc.* **2016**, *138*, 3022 – 3030.
[19] S. Yang, A. J. Ramirez-Cuesta, R. Newby, V. Garcia-Sakai, P. Manuel, S. K. Callear, S. I. Campbell, C. C. Tang, M. Schröder, *Nat. Chem.* **2015**, *7*, 121 – 129.
[20] K.-J. Chen, H. S. Scott, D. G. Madden, T. Pham, A. Kumar, A. Bajpai, M. Lusi, K. A. Forrest, B. Space, J. J. Perry, M. J. Zaworotko, *Chem* **2016**, *1*, 753 – 765.
[21] Y.-L. Peng, T. Pham, P. Li, T. Wang, Y. Chen, K.-J. Chen, K. A. Forrest, B. Space, P. Cheng, M. J. Zaworotko, Z. Zhang, *Angew. Chem. Int. Ed.* **2018**, *57*, 10971 – 10975; *Angew. Chem.* **2018**, *130*, 11137 – 11141.
[22] F. Luo, C. Yan, L. Dang, R. Krishna, W. Zhou, H. Wu, X. Dong, Y. Han, T.-L. Hu, M. O'Keeffe, L. Wang, M. Luo, R.-B. Lin, B. Chen, *J. Am. Chem. Soc.* **2016**, *138*, 5678 – 5684.
[23] S. C. Xiang, W. Zhou, Z. J. Zhang, M. A. Green, Y. Liu, B. L. Chen, *Angew. Chem. Int. Ed.* **2010**, *49*, 4615 – 4618; *Angew. Chem.* **2010**, *122*, 4719 – 4722.
[24] S. Bureekaew, H. Sato, R. Matsuda, Y. Kubota, R. Hirose, J. Kim, K. Kato, M. Takata, S. Kitagawa, *Angew. Chem. Int. Ed.* **2010**, *49*, 7660 – 7664; *Angew. Chem.* **2010**, *122*, 7826 – 7830.
[25] a) R. Krishna, B. Smit, S. Calero, *Chem. Soc. Rev.* **2002**, *31*, 185 – 194; b) B. Liu, B. Smit, *Langmuir* **2009**, *25*, 5918 – 5926; c) J. Duan, M. Higuchi, R. Krishna, T. Kiyonaga, Y. Tsutsumi, Y. Sato, Y. Kubota, M. Takata, S. Kitagawa, *Chem. Sci.* **2014**, *5*, 660 – 666.
[26] R. Matsuda, R. Kitaura, S. Kitagawa, Y. Kubota, R. V. Belosludov, T. C. Kobayashi, H. Sakamoto, T. Chiba, M. Takata, Y. Kawazoe, Y. Mita, *Nature* **2005**, *436*, 238 – 241.

Manuscript received: April 4, 2019
Accepted manuscript online: April 17, 2019
Version of record online: May 9, 2019

Angewandte Chemie
Eine Zeitschrift der Gesellschaft Deutscher Chemiker

Supporting Information

Induced Fit of C_2H_2 in a Flexible MOF Through Cooperative Action of Open Metal Sites

Heng Zeng, Mo Xie, Yong-Liang Huang, Yifang Zhao, Xiao-Jing Xie, Jian-Ping Bai, Meng-Yan Wan, Rajamani Krishna, Weigang Lu, and Dan Li**

ange_201904160_sm_miscellaneous_information.pdf

Materials and Methods

General Methods.

All reagents and starting materials were obtained commercially and used as received without any further purification. $Zn(NO_3)_2 \cdot 6H_2O$ and Benzotriazole-5-carboxylic acid (H_2btca) were purchased from Sinopharm Chemical Reagent Co. Ltd. Ultrahigh-purity-grade (>99.999%) N_2, CO_2, and C_2H_2 gases were used for adsorption-related measurements. Thermogravimetric analysis was performed under a N_2 atmosphere with a temperature increasing at a rate of 10 ^oC min^{-1} on a TA-Q50 system.

Synthesis of JNU-1.

A mixture of $Zn(NO_3)_2 \cdot 6H_2O$ (0.1 mmol, 24.9 mg), H_2btca (0.05 mmol, 8.0 mg), DMF (3.0 mL), and H_2O (1.0 mL) was placed into a Pyrex glass tube and heated to 140 ^oC for three days. After cooled to room temperature, the block-shaped yellowish crystals were collected and washed with DMF three times.

Single-component gas adsorption.

At least 100 mg of sample was used for each measurement. **JNU-1** was desolvated at 200 ^oC under dynamic vacuum (below 5 μmHg) for 36 h. Single-component gas adsorption isotherms were measured on an ASAP 2020 PLUS Analyzer (Micromeritics).

The isosteric enthalpy of adsorption (Q_{st}).

The isosteric enthalpy of adsorption for C_2H_2 and CO_2 were calculated using the gas adsorption data collected at 273 and 298 K. The adsorption curves were first fitted with the dual-site Langmuir-Freundlich (DSLF) equation[1], subsequently the Clausius-Clapeyron method[2] were used to calculate Q_{st} . The DSLF equation is given as:

$$q = q_{A,sat}\frac{b_A P^{1/nA}}{1 + b_A P^{1/nA}} + q_{B,sat}\frac{b_B P^{1/nB}}{1 + b_B P^{1/nB}}$$

Where q is gas uptake (in mmol g^{-1}), *P* is pressure (in kPa), $q_{A,sat}$ and $q_{B,sat}$ are saturation uptakes (in mmol g^{-1}) for sites 1 and 2, b_A and b_B are affinity coefficients (in kPa^{-1}) for sites 1 and 2, and nA and nB represent the deviations from the ideal homogeneous surface for sites 1 and 2. The parameters that were obtained from the fitting of the C_2H_2 and CO_2 adsorption isotherms can be found in Tables S1. All isotherms were fitted with $R^2 > 0.999$.

The obtained parameters were used to calculate Q_{st} in the range of adsorption capacity through the Clausius-Clapeyron equation, which is as follows:

$$Q_{st} = -R\frac{\partial \ln P}{\partial(1/T)}$$

Where T is temperature (in K) and R is the ideal gas constant. The partial derivative term represents the slope of the plot of ln *P vs.* 1/T for a number of isotherms at different temperatures and various loadings. Therefore, the above Q_{st} equation can be simplified as:

$$Q_{st} = -mR$$

Where m is the slope, which can be calculated by the following equation with three different temperatures and their corresponding pressures:

$$m = \frac{\Sigma \frac{1}{T_i} \ln P_i - \frac{1}{3}(\Sigma \frac{1}{T_i})(\Sigma \ln P_i)}{\Sigma \left(\frac{1}{T_i}\right)^2 - \frac{1}{3}(\Sigma \frac{1}{T_i})^2}$$

The P_i values were back-calculated for a range of uptakes using the DSLF equation via an iterative technique (e.g., the Newton-Raphson method)[3].

Single Crystal X-ray diffraction structure analysis.

Single crystal diffraction data of desolvated **JNU-1**, **CO_2@JNU-1** and **C_2H_2@JNU-1** were collected at room temperature and at 150 K, respectively, *via* an Oxford Cryo stream system on a XtaLAB PRO MM007-DW diffractometer system equipped with a RA-Micro7HF-MR-DW(Cu/Mo) X-ray generator and Pilatus3R-200K-A detector (Rigaku, Japan, Cu Kα, λ = 1.54178 Å). The structures were solved and refined using Olex2 with 'XS' and 'XL' plug-in. The activated **JNU-1** crystals were filled with acetylene via an acetylene balloon at room temperature. A single crystal of **C_2H_2@JNU-1** and **CO_2@JNU-1** were covered with Paratone-N oil, mounted onto a loop, transferred to diffractometer, and then single crystal x-ray diffraction (SCXRD) data were collected under N_2 flow (**Table S4**).

Powder X-ray diffraction (PXRD) analysis.

Powder x-ray diffraction data was collected using microcrystalline samples on a Rigaku Ultima IV diffractometer (40 kV, 40 mA, CuKα1, 2λ = 1.5418 Å). The measurement parameters include a scan speed of 10 (°)/min, a step size of 0.02 (°), and a scan range of 2θ from 5(°) to 30(°). For Temperature-dependent PXRD, the measurement parameters include a scan speed of 2 °C/min, a step size of 0.02(°), and a scan range of 2θ from 5(°) to 30(°). For *in situ* adsorption coupled with X-ray diffraction experiments, carbon dioxide or acetylene partial pressure was controlled by changing the ratio of CO_2/N_2 or C_2H_2/N_2.

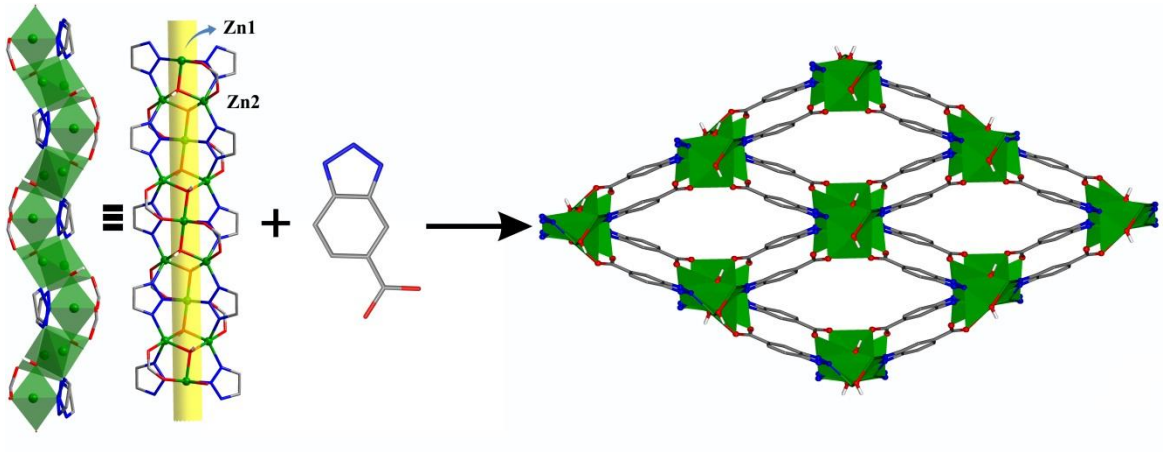

Figure S1. Schematic diagram of construction of **JNU-1** (H atoms are not shown for clarity). General color code: Zn, green; N, turquoise; O, red; C, gray.

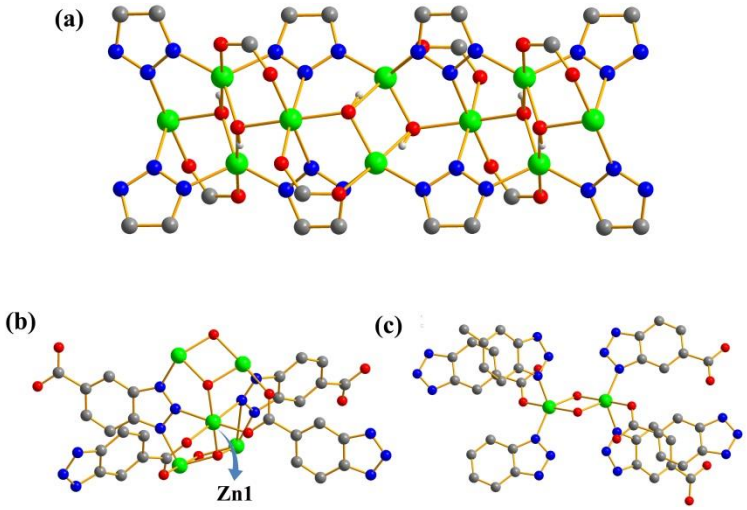

Figure S2. (a) Zn-O chain in **JNU-1** showing two crystallgraphically different Zn centers. The coordination environments of (b) Zn1 and (c) Zn2.

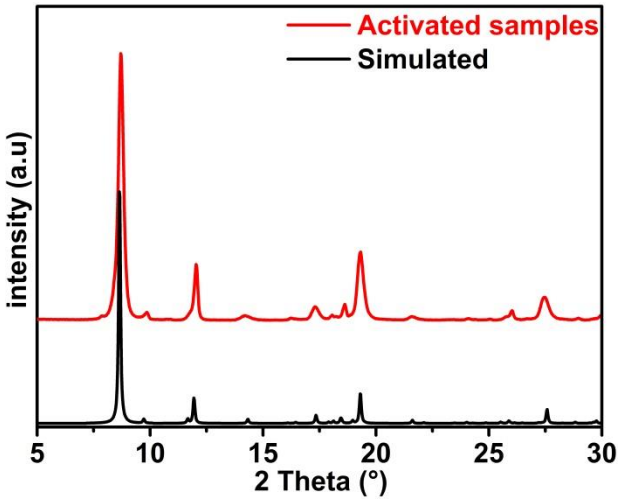

Figure S3. PXRD patterns of the simulated (black) and activated (red) **JNU-1**.

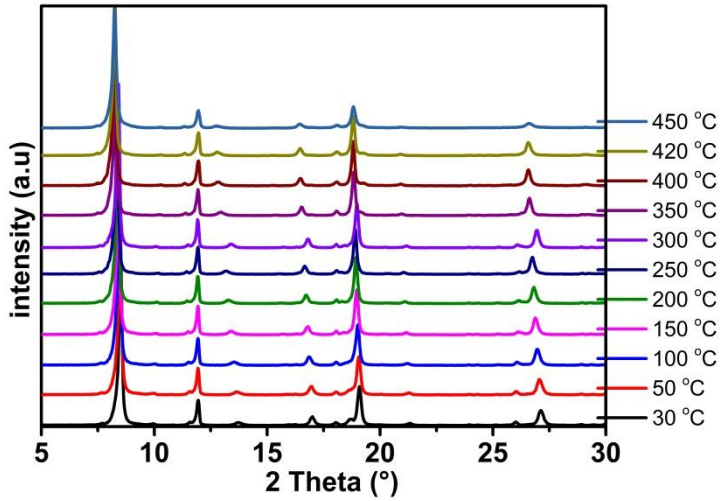

Figure S4. *In-situ* variable-temperature PXRD (VT-PXRD) patterns of **JNU-1** under a N_2 atmosphere.

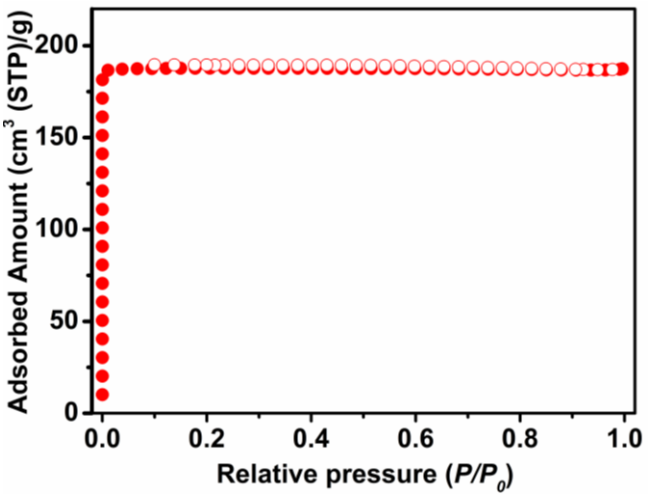

Figure S5. N_2 adsorption/desorption isotherm of **JNU-1** at 77K.

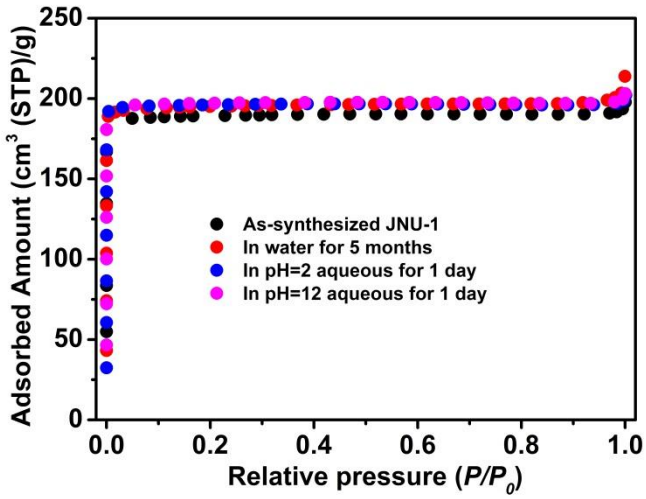

Figure S6. N_2 adsorption isotherms of **JNU-1** at 77K. As-synthesized **JNU-1** (black), soaked in water for 5 months (red), soaked in aqueous solution (pH=2) for one day (blue), soaked in aqueous solution (pH=12) for one day (magenta).

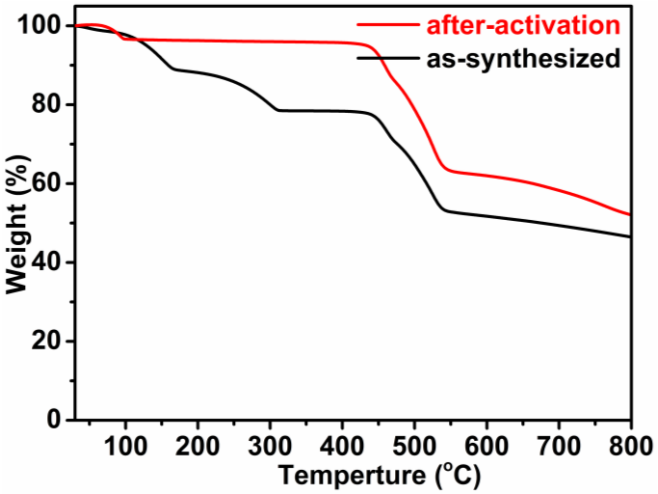

Figure S7. Thermogravimetric analysis (TGA) curves of the as-synthesized and activated samples of **JNU-1**.

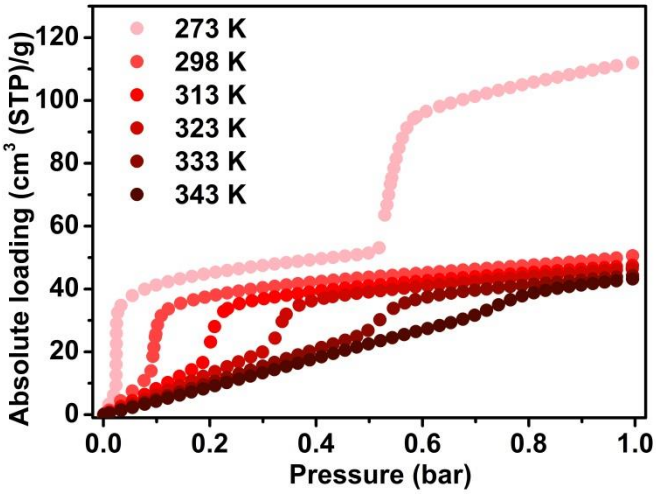

Figure S8. CO_2 adsorption isotherms of **JNU-1** at different temperatures.

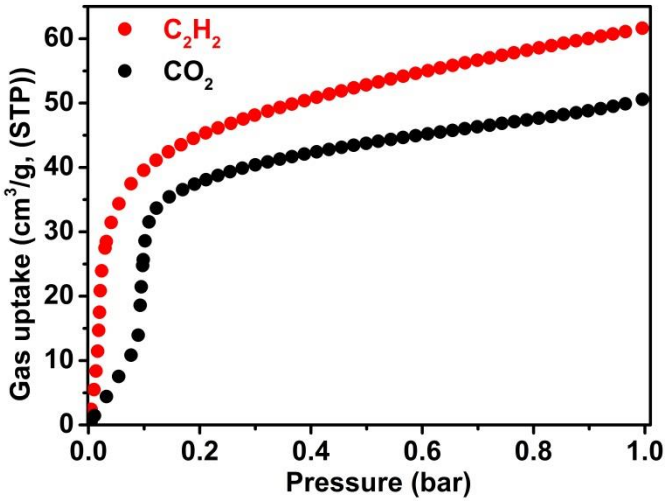

Figure S9. C_2H_2 and CO_2 gas adsorption isotherms of **JNU-1** at 298 K.

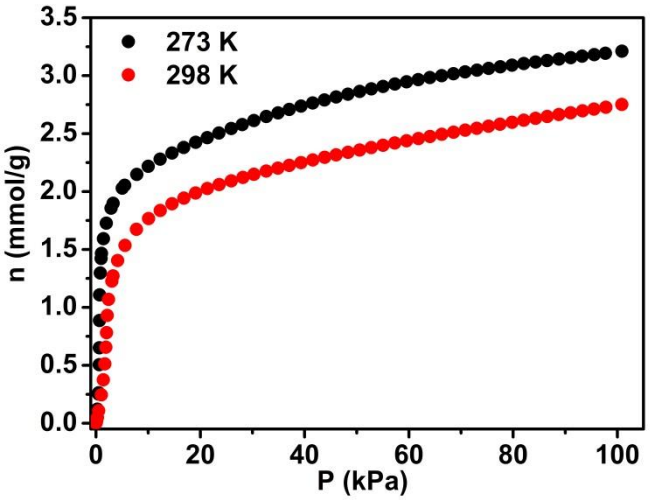

Figure S10. C_2H_2 adsorption isotherms of **JNU-1** at 273K and 298K.

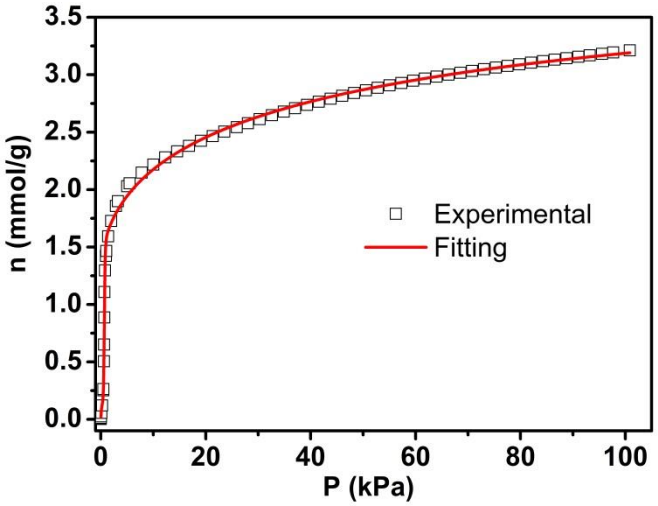

Figure S11. Dual-site Langmuir-Freundlich fitting of the C_2H_2 adsorption isotherm of **JNU-1** at 273 K.

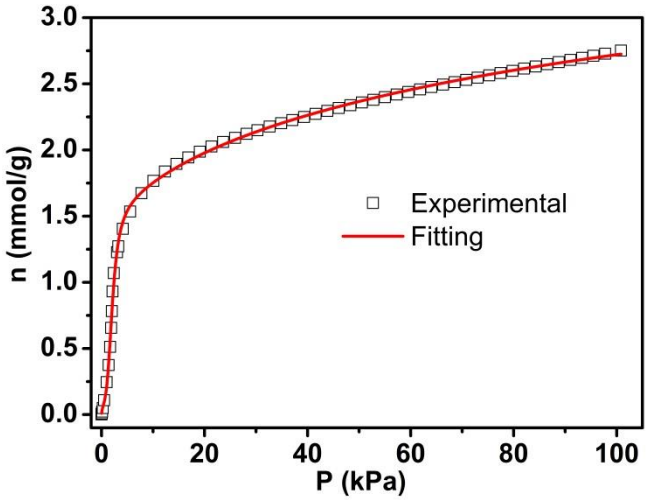

Figure S12. Dual-site Langmuir-Freundlich fitting of the C_2H_2 adsorption isotherm of **JNU-1** at 298 K.

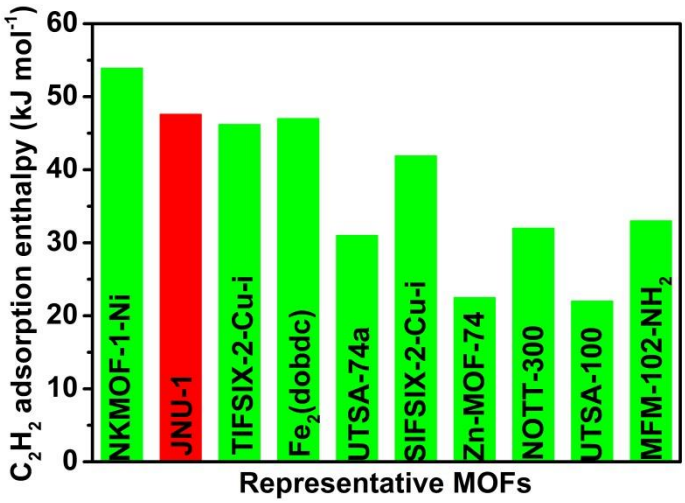

Figure S13. The maximum adsorption enthalpy of C_2H_2 on **JNU-1** and some selected MOFs.

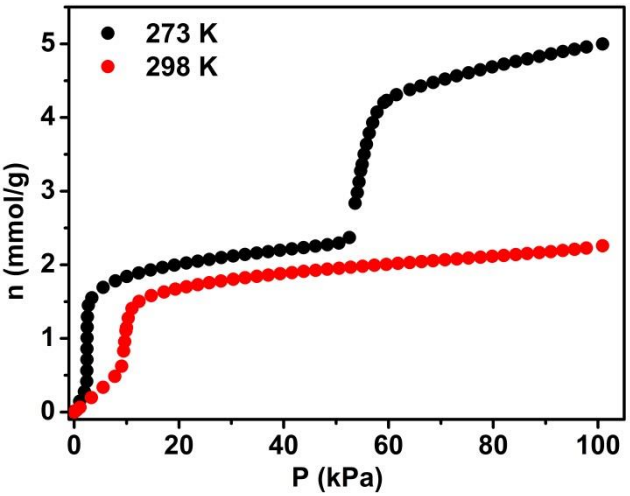

Figure S14. CO_2 adsorption isotherms of **JNU-1** at 273K and 298K.

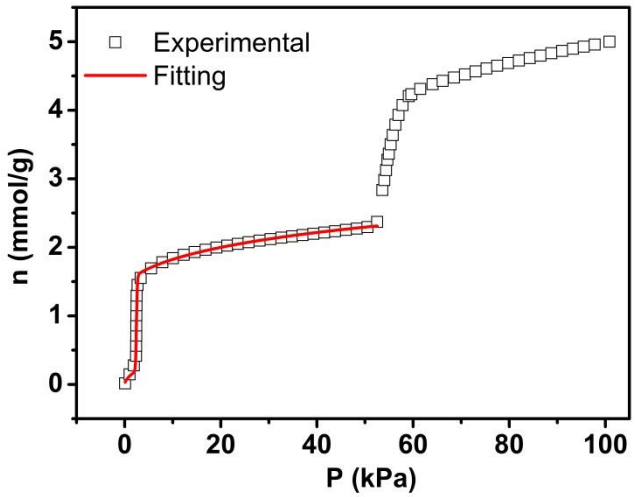

Figure S15. Dual-site Langmuir-Freundlich fitting of the CO_2 adsorption isotherm of **JNU-1** at 273 K (0 - 50 kPa).

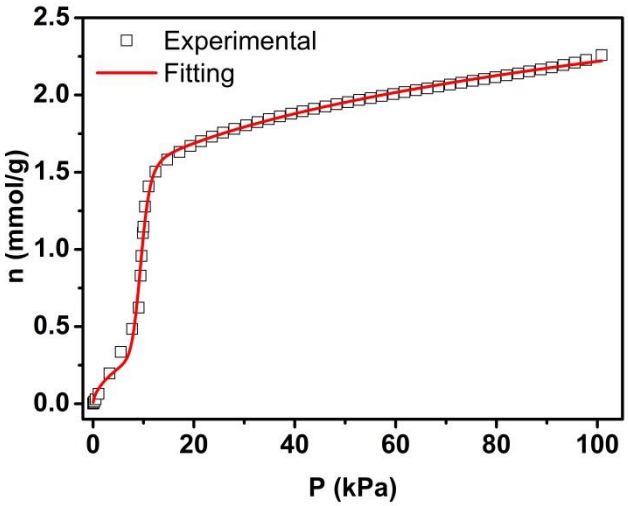

Figure S16. Dual-site Langmuir-Freundlich fitting of the CO_2 adsorption isotherm of **JNU-1** at 298 K.

Table S1. Dual-site Langmuir-Freundlich parameters from the fitting of C_2H_2 adsorption isotherms of **JNU-1** at 273 and 298 K. The R^2 values are also provided.

Parameter	**273K**	**298K**
$q_{A,sat}$	3.129	3.434
b_A	0.0973	0.0399
n_A	1.685	1.572
$q_{B,sat}$	1.311	1.251
b_B	34.686	0.0710
n_B	0.109	0.281
R^2	0.998	0.999

Table S2. Dual-site Langmuir-Freundlich parameters from the fitting of CO_2 adsorption isotherms of **JNU-1** at 273 and 298 K. The R^2 values are also provided.

Parameter	**273K**	**298K**
$q_{A,sat}$	2.455	3.689
b_A	0.0508	0.026
n_A	1.607	1.728
$q_{B,sat}$	1.393	1.214
b_B	3.315×10^{-11}	4.196×10^{-11}
n_B	0.0373	0.0942
R^2	0.98	0.998

IAST calculations of adsorption selectivity.

In order to establish the feasibility of C_2H_2/CO_2 separations we performed calculations using the Ideal Adsorbed Solution Theory (IAST) of Myers and Prausnitz[4].

The adsorption selectivity, Sads, defined for separation of a binary mixture of species i and j by

$$S_{ads} = \frac{q_i/q_j}{p_i/p_j}$$

where the q_i represent the molar loadings of component i that is in equilibrium with a bulk gas phase with partial pressures p_i in the mixture.

Table S3. Dual-site Langmuir-Freundlich parameters from the fitting of C_2H_2 and CO_2 adsorption isotherms of **JNU-1** at 298 K. The R^2 values are also provided.

Parameter	**C_2H_2**	**CO_2**
$q_{A,sat}$	3.434	3.689
b_A	0.0399	0.026
n_A	1.572	1.728
$q_{B,sat}$	1.251	1.214
b_B	0.0710	4.196×10^{-11}
n_B	0.281	0.0942
R^2	0.999	0.998

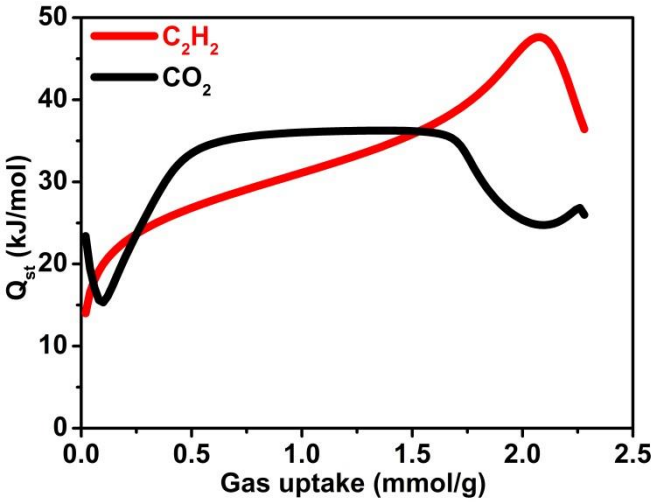

Figure S17. Heats of adsorption of both C_2H_2 and CO_2 in **JNU-1**.

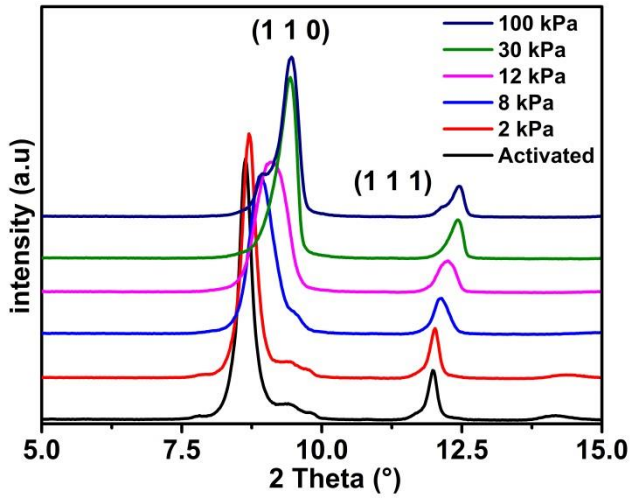

Figure S18. *In situ* PXRD patterns of **JNU-1** in different C_2H_2 concentrations at 298 K.

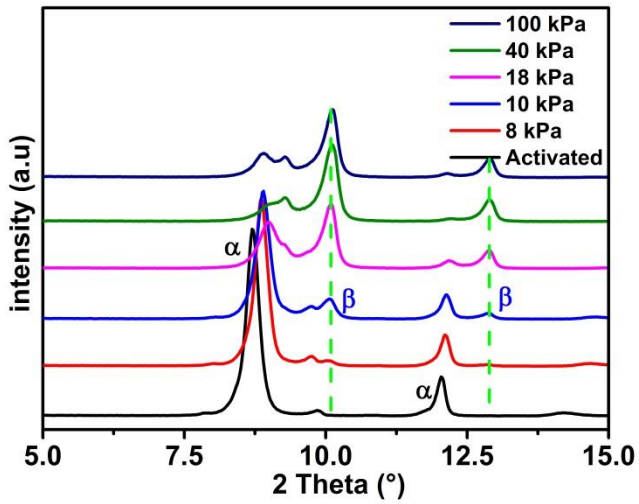

Figure S19. *In situ* PXRD patterns of **JNU-1** in different CO_2 concentrations at 298 K.

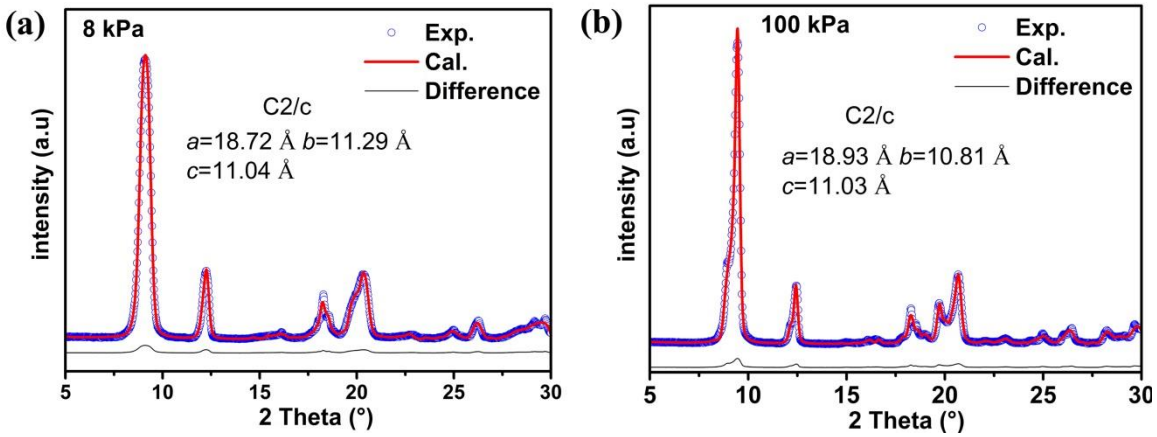

Figure S20. Observed (blue) and calculated (red) PXRD profiles and difference plot [I_{obs}-I_{calc}] (grey) of the Pawley[5] refinement of **JNU-1** (2θ range 5.0 - 30.0°, dmin = 1.2Å).

Computational method

The adsorption sites of **C_2H_2@JNU-1** were calculated using period DFT methods as in the CASTEP module embedded the Material Studio 2018 software. Calculations were performed under the Perdew-ang exchange and correlation functional[6] with a plane-wave energy cutoff of 351 eV. The lattice parameters and atomic coordinated determined by XRD were used for the initial structure for optimization and only Gamma centered grid were used for the unit cell. Note that all the calculations were performed at 298 K, so the adsorption sites in the simulated **C_2H_2@JNU-1** are slightly moved away from the open Zn(II) sites compared to the observed adsorption sites in single crystal of **C_2H_2@JNU-1** solved at 150 K (**Figure S20**).

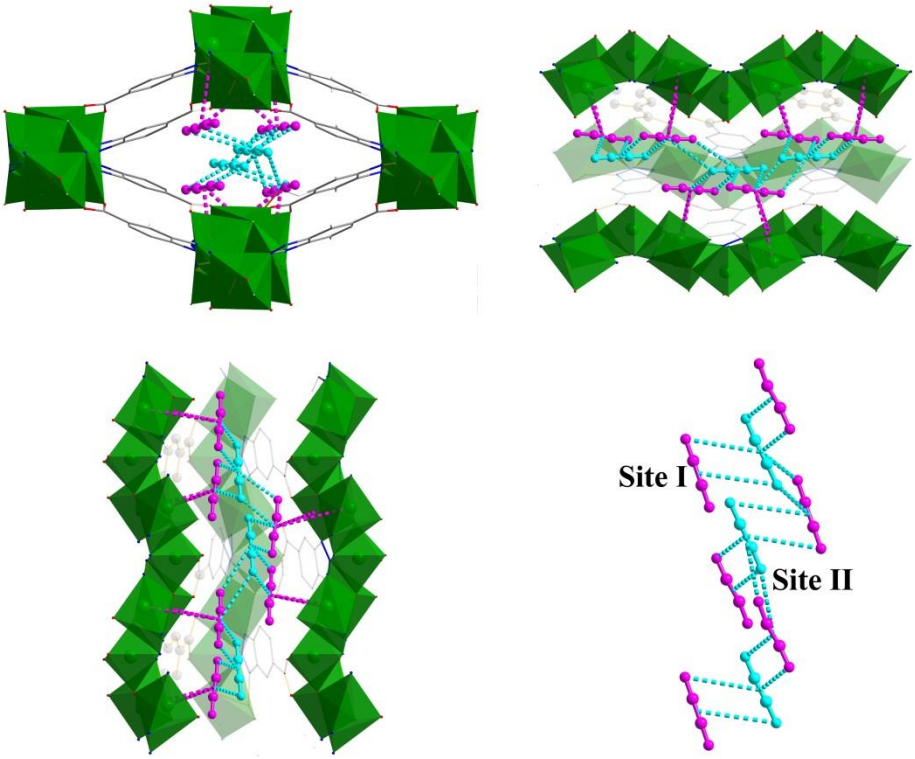

Figure S21. View of the binding sites for C_2H_2 molecules (C_2H_2 molecules in space-filling mode) from molecular simulations.

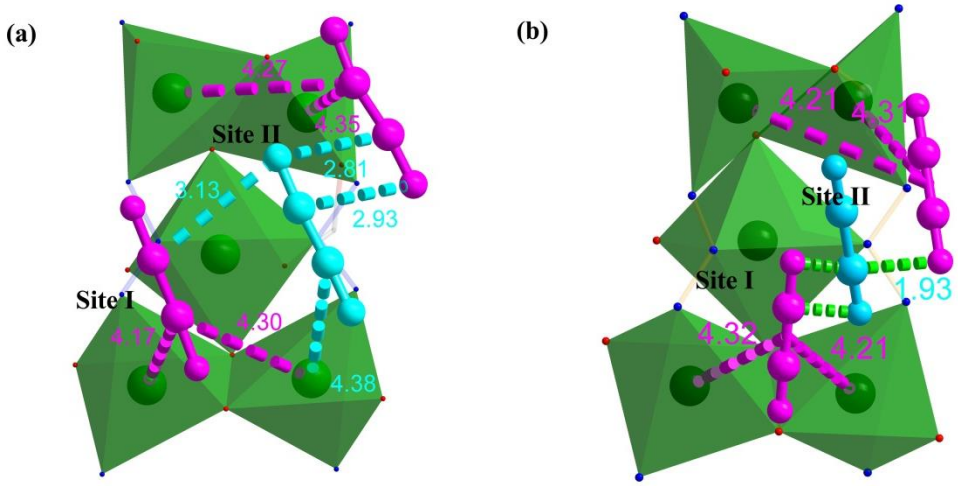

Figure S22. (a) Two binding sites (I, II) for C_2H_2 in **JNU-1** determined by molecular modeling study. (b) Two binding sites (I, II) for C_2H_2 in **JNU-1** determined by single-crystal structure of **C_2H_2@JNU-1**, viewed along the *b* axis.

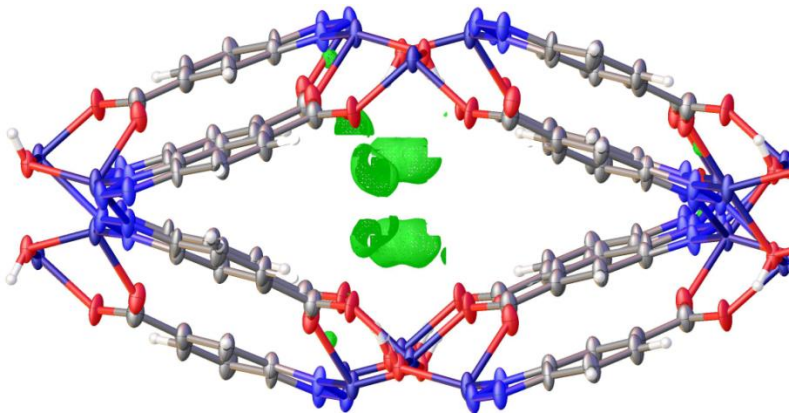

Figure S23. 3D electron density maps (F_o–F_c contoured at 2.7 e $Å^{-3}$ in green) of CO_2-loaded **JNU-1**.

Column Breakthrough Experiments.

The mixed-gas breakthrough separation experiment was conducted under ambient conditions (298K, 1 atm) by using a lab-scale fixed-bed system (**Figure S24**). In a typical breakthrough experiment for a C_2H_2/CO_2 (50:50, v/v) gas mixture, **JNU-1** powder (2.2 g) was packed into a quartz column (8.0 mm I.D. × 450 mm) with silica wool filling the void space. The sorbent was activated in-situ in the column at 393 K with a high vacuum for 24 h. After the activation process, a helium flow (100 cm^3 min^{-1}) was introduced to purge the adsorbent. The flow of He was then turned off and a gas mixture of C_2H_2/CO_2 (2 cm^3 min^{-1}) was allowed to flow into the column. Outlet effluent from the column was continuously monitored using gas chromatography (GC-7890B, Agilent) with a thermal conductivity detector (TCD). After the breakthrough experiment, the sample was regenerated with helium flow (100 cm^3 min^{-1}) at 393 K for 2 h. The complete breakthrough of C_2H_2 was indicated by the downstream gas composition reaching that of the feed gas. On the basis of the mass balance, the gas adsorption capacities can be determined as follows:[7]

$$q_i = \frac{C_i V}{22.4 \times m} \times \int_0^t (1 - \frac{F}{F_0})\, dt$$

Where q_i is the equilibrium adsorption capacity of gas i (mmol g^{-1}), C_i is the feed gas concentration, V is the volumetric feed flow rate (cm^3 min^{-1}), t is the adsorption time (min), F_0 and F are the inlet and outlet gas molar flow rates, respectively, and m is the mass of the adsorbent (g). The separation factor (α) of the breakthrough experiment is determined as:

$$\alpha = \frac{q_A y_B}{q_B y_A}$$

in which y_i is the molar fraction of gas *i* (*i* = A, B) in the gas mixture.

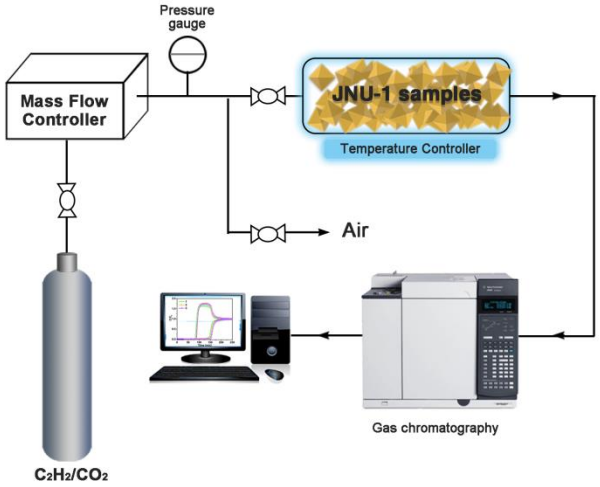

Figure S24. Schematic illustration of the apparatus for the breakthrough experiments.

Table S3. Summary of the adsorption capacity of C_2H_2 and CO_2, as well as C_2H_2/CO_2 (1/1) selectivity in some selected MOFs (reorganized from ref. S11-S13).

MOFs	**C_2H_2 (cm^3/g, STP)**	**CO_2 (cm^3/g, STP)**	**C_2H_2/CO_2 (1/1) selectivity**	**Condition**	**Ref**
$[Cu_2(pzdc)_2(pyz)]$	42	4	10.5	270 K, 4.5 kPa	8
MAF-2	70	19	3.68	298 K, 100 kPa	9
HKUST-1	201	113	1.78	~298 K, 100 kPa	10
$Mg(HCOO)_2$	66	45	1.47	298 K, 100 kPa	11
UTSA-74-Zn	108.2	70.9	1.53	296 K, 100 kPa	12
SIFSIX-1-Cu	190.4	107.9	1.74	298 K, 100 kPa	13
SIFSIX-2-Cu-i	108.4	90.0	1.21	298 K, 100 kPa	12
SIFSIX-3-Zn	81.5	57.0	1.43	273K, 91 kPa	12
[Mn(bdc)(dpe)]	7.3	46.8	0.156	298 K, 100 kPa	14
UTSA-300a	68.9	3.25	21	298 K, 100 kPa	15
Mg-MOF-74	184.4	179.2	1.03		16
JCM-1	76.5	38.1	2.01	298 K, 100 kPa	17
JNU-1	**27.4**	**4.1**	**6.6**	**298 K, 3 kPa**	**This work**

Table S4. Crystal data of **desolvated JNU-1**, **C_2H_2@JNU-1** and **CO_2@JNU-1** (desolvated **JNU-1** exposed to atmospheric C_2H_2 gas for several hours).

	Desolvated JNU-1	**C_2H_2@JNU-1**	**CO_2@JNU-1**
Formula	$C_{14}H_8N_6O_6Zn_3$	$C_{35}H_{23}N_{12}O_{12}Zn_6$	C14H8N6O6Zn3,Q
CCDC number	1890470	1890464	1907749
Space group	C2/c	C2/c	C2/c
Crystal system	monoclinic	monoclinic	monoclinic
a (Å)	18.1932(4)	19.1285(14)	19.1274(7)
b (Å)	12.35(3)	10.2763(11)	10.2305(5)
c (Å)	11.01(2)	11.0671(6)	11.0676(3)
α (deg)	90	90	90
β (deg)	92.344	90.328	90.297
γ (deg)	90	90	90
V (Å)^3	2472.93	2175.4	2165.71
Z	4	2	4
ρ calcg/cm^3	1.484	1.826	1.878
μ/mm^{-1}	3.72	4.28	4.24
Final R	R1=0.0373	R1=0.064	R1=0.071
[I>2sigma (I)]	wR1=0.0941	wR1=0.191	wR1=0.203
GooF	0.956	1.109	1.058
Completeness	100%	92%	99%

1. R. T. Yang, Gas Separation by Adsorption Processes; Imperial College Press: London, **1986**.

2. H.; Pan, J. A. Ritter, P. B. Balbuena, *Langmuir* **1998**, *14*, 6323-6327.

3. E. T. Whittaker, G. Robinson, The Calculus of Observations: A Treatise on Numerical Mathematics, 4th Ed.; Dover: New York, **1967**, 84-87.

4 A.L. Myers, J.M. Prausnitz, Thermodynamics of mixed-gas adsorption. *AIChE J*. **1965**, *11*, 121-127.

5. G. S. Pawley, *J. Appl. Cryst.* **1981**, *14*, 357-361.

6. J. P. Perdew, K. Burke, Y. Wang, *Phys. Rev. B* **1996**, *54*, 16533-16539.

7. J. Liu, J. Tian, P. K. Thallapally, B. P. McGrail, *J. Phys. Chem. C* **2012**, *116*, 9575-9581.

8. R. Matsuda, R. Kitaura, S. Kitagawa, Y. Kubota, R. V. Belosludov, T. C. Kobayashi, H. Sakamoto, T. Chiba, M. Takata, Y. Kawazoe, Y. Mita, *Nature* **2005**, *436*, 238.

9. J.-P. Zhang, X.-M. Chen, *J. Am. Chem. Soc.* **2009**, *131*, 5516.

10. M. Fischer, F. Hoffmann, M. Fröba, *ChemPhysChem* **2010**, *11*, 2220.

11. H. Kim, D. G. Samsonenko, M. Yoon, J. W. Yoon, Y. K. Hwang, J.-S. Chang, K. Kim, *Chem. Comm.* **2008**, 4697.

12. F. Luo, C. Yan, L. Dang, R. Krishna, W. Zhou, H. Wu, X. Dong, Y. Han, T.-L. Hu, M. O'Keeffe, L. Wang, M. Luo, R.-B. Lin, B. Chen, *J. Am. Chem. Soc.* **2016**, *138*, 5678.

13. X. Cui, K. Chen, H. Xing, Q. Yang, R. Krishna, Z. Bao, H. Wu, W. Zhou, X. Dong, Y. Han, B. Li, Q. Ren, M. J. Zaworotko, B. Chen, *Science* **2016**, *353*, 141.

14. M. L. Foo, R. Matsuda, Y. Hijikata, R. Krishna, H. Sato, S. Horike, A. Hori, J. Duan, Y. Sato, Y. Kubota, M. Takata, S. Kitagawa, *J. Am. Chem. Soc.* **2016**, *138*, 3022.

15. R. B. Lin, L. Li, H. Wu, H. Arman, B. Li, R. G. Lin, W. Zhou, B. Chen, *J. Am. Chem. Soc.* **2017**, *139*, 8022-8028.

16. (a) S. R. Caskey, A. G. Wong-Foy, A. J. Matzger, *J. Am. Chem. Soc.* **2008**, *130*, 10870-10871; (b) S. Xiang, W. Zhou, Z. Zhang, M. A. Green, Y. Liu, Chen, B. *Angew. Chem. Int. Ed. Engl.* **2010**, *49*, 4615-4618.

17. J. Lee, C. Y. Chuah, J. Kim, Y. Kim, N. Ko, Y. Y. Seo, K. Kim, T. H. Bae, E. Lee, *Angew. Chem., Int. Ed.* **2018**, *57*, 7869-7873.